Hindawi
Shock and Vibration
Volume 2019, Article ID 9674274, 16 pages
https://doi.org/10.1155/2019/9674274

Research Article

Experimental and Numerical Investigations of Pressure Field of Curved Shell Structure Subjected to Interior Blast

Jialu Ma,[1] **Feng Fan**,[2] **Lingxin Zhang**,[1] **Chengqing Wu**,[3] **and Xudong Zhi**[2]

[1]*Institute of Engineering Mechanics, China Earthquake Administration, Harbin 150080, China*
[2]*School of Civil Engineering, Harbin Institute of Technology, Harbin 150090, China*
[3]*School of Civil and Environmental Engineering, University of Technology Sydney, Ultimo, NSW 2007, Australia*

Correspondence should be addressed to Xudong Zhi; zhixudong@hit.edu.cn

Received 25 April 2019; Revised 9 July 2019; Accepted 22 July 2019; Published 21 August 2019

Academic Editor: Stefano Manzoni

A terrorist attack on a long-span spatial structure would cause horrible results. Therefore, it is important to determine the characteristics of blast pressure fields to protect such structures. In this study, fully confined blast loading tests were conducted using a rigid curved shell model, which had an inner space similar to that of a reticulated dome. Four different scenarios were carried out to record the blast loading on five typical positions. The blast pressure-time data were compared and analyzed. In addition, a suitable numerical simulation method was proposed for the issues involved in interior blast loading. This numerical model was verified by comparing with the test data. A parametrical analysis of the interior blast simulations was conducted based on this numerical method. The blast loading values at specific positions were obtained with the key parameters varied within a reasonable scope. The blast loading from blast tests and simulations were presented. On this basis, the interior blast loading could conveniently be predicted by using the method and data in this paper, which could be used in the protective design of other reticulated domes.

1. Introduction

Long-span spatial structures with graceful configurations are always considered to be city landmarks. A terrorist attack on such a structure would not only cause a huge economic loss, but would also cause many injuries. Therefore, it is important to consider blast protective measures during the structural design period.

Over the last century, numerous studies have been performed on blast loading. The US army presented the most authoritative guideline (UFC 3-340-02) [1], which was improved based on TM5-1300. It includes many blast issues with multiple situations regarding different structural types and shapes. The UFC guideline systemically presents figures and tables that can be used for predicting the blast loading in some typical situations. However, the UFC guideline lacks information about special cases, which should be studied with extra specialized research using blast tests and numerical simulations. Wu and Hao conducted a series of blast tests with different explosive parameters [2–5]. Yang et al. and Bao et al. used many detailed features to compare the difference between TNT explosives and combustible gas [6, 7]. The blast propagation and reflection in a complicated community was simulated with LS-DYNA by Li and Shi [8–11]. Some studies relating to long-span spatial structures were also conducted by Gao and Wang using fluid-structure interaction (FSI) methods [12]. The exterior blast loading and failure of reticulated domes were studied by Xudong et al. and Zhi et al. [13, 14]. Ma et al. had investigated the blast distribution numerically [15, 16], and the failure modes and failure mechanisms were developed [17, 18]. However, the blast loading on a long-span spatial structure is not clear and verified in the existing references, which is important for the protective design of structures.

In this study, single-layer reticulated domes, which are the most common type of long-span spatial structures, were taken as examples to investigate the pressure field distributions when subjected to an interior blast. A series of blast tests to examine the pressure distribution in a curved shell were designed and performed. The blast loading values on

five points, which represented the typical positions of the reticulated domes, were recorded with different TNT equivalences. In addition, suitable finite element (FE) models were set up. Blast tests that included the detonation, propagation, and reflection were simulated and verified by comparing the results to the recorded test data for the corresponding positions. Based on the numerical models, a parameter analysis was conducted to calculate the blast loading values of some standard cases, which could conveniently be used to estimate the blast loading values at specific positions for similar domes subjected to an interior blast.

2. Setup of Blast Tests

To investigate the interior blast loading of the reticulated domes, a series of blast tests were conducted. According the conclusions in reference [15], the blast loading obtained from the rigid model could be used when investigating the blast issues related to the large-scaled distances involved in long-span spatial structures. Thus, a fully confined curved steel shell model was used to simulate the inside environment of a reticulated dome, and some pressure gauges were placed on the model to record the pressure-time history data at five typical positions.

An almost rigid steel shell with a 1 m span was designed as shown in Figure 1. The steel model had a thickness of 0.03 m, and its rise-span ratio was 1/5. In addition, the substructure wall was also considered in the rigid shell model. The total height of the curved shell model was 0.57 m, which included a 0.2 m roof rise and a 0.37 m support wall, as shown in Figure 2. TNT explosives were detonated in the center of the model at ground level during the tests. PCB pressure gauges (PCB102B04 and PCB102B06) were used, which had maximum measurement ranges of 3450 kPa and 6900 kPa, respectively. In addition, the model had five holes for installing the pressure gauges. The P-3 gauge was installed in the middle, with the other gauges installed symmetrically. These were used to compare and verify the records for the quartile and corner positions. The ignition device (WY2) and monitor (DH5927) were used to detonate the explosive and record the pressure data, respectively.

The curved shell model was composed of three parts, including the top rigid shell, basement plate, and connection system, as shown in Figure 3. During the tests, the model was nearly airtight because of the weight of the top shell. In addition, the 28 high-strength bolts in the connection system could sustain no less than approximately 5.04 MPa of dynamic action. With the goal of maintaining the original blast loading distribution, the inside surface of the top model was polished and painted before the tests. The TNT and exploders were placed at the center of the basement plate to detonate during the experiments. Moreover, a replaceable 10 mm thick steel sheet was located under the explosives to keep the connected surface flat before each test.

The weights of the TNT explosives from the laboratory were 200 g and 400 g, which had to be cut to a suitable weight for each test. It was difficult to reshape the TNT into a hemispherical shape. Therefore, a TNT cube was used instead. After the TNT and exploder were prepared and placed, all of the gauges were checked and calibrated before the tests. The exploder was electrically detonated by the WY2 ignition device, which could also trigger the monitoring system at the same time. The final preparation of the pressure measurement tests is shown in Figure 4.

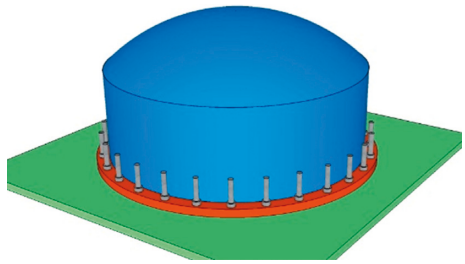

Figure 1: Design model of curved shell structure.

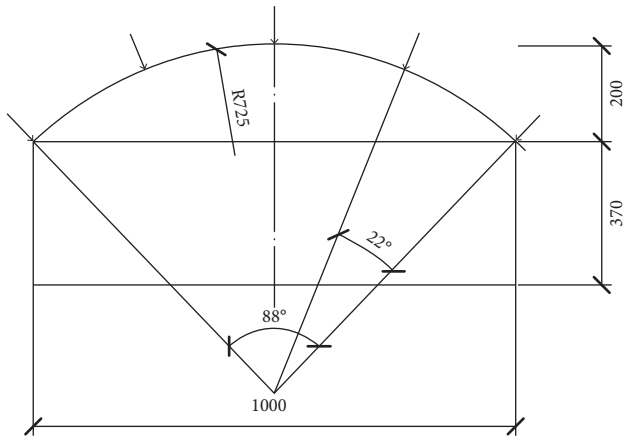

Figure 2: Model dimensions and gauge positions (units: mm).

Figure 3: Test model components.

3. Blast Loading Data from Tests

For the blast tests, the scaled distance is defined in the following equation [19]:

Figure 4: Test model for interior blast loading.

$$Z = \frac{R}{W^{1/3}}, \quad (1)$$

where R is the stand-off distance, and W is the TNT explosive equivalent.

Within the scope of an interior blast occurring in a spatial structure, it is difficult for a person to carry a large equivalence of explosives past security checks. Therefore, the pressure measurement tests only focused on large-scaled distance cases, which involved values larger than 2 m/kg$^{1/3}$ in this work. Thus, a series of blast tests were conducted with four scenarios and different TNT equivalences: 8 g, 13 g, 18 g, and 23 g. It should be noted that the exploder was also considered to be 3 g of TNT in the total equivalences listed in Table 1.

During the tests, there were no obviously different phenomena observed from outside of the model, with the exception of the volume values for the explosion sounds. In addition, it is known that blast actions vanish in very short periods. The relatively long-period quasistatic gas pressures were quite different from the shock waves, as shown in Figure 5. Even within the real situations of spatial structures, the gas would gradually be vented from the doors and windows. Therefore, the shock period was more meaningful in this research. During the blast recording time of the tests, there was almost no visible smoke leakage, which showed that the model was airtight during the blast monitoring period. This meant the shock pressure data could be treated as an ideal fully confined blast process without leakage. However, it was still difficult to watch the phenomena of the shock waves propagating inside the rigid shell model. The evolution of the blast loading could generally be deduced from the data recorded by the five pressure gauges. In the following subsections, the test data are analyzed and compared by scenario.

3.1. Scenario T1. In scenario T1, the total TNT equivalence, including the exploder, was 8 g. The scaled distance was 2.850 m/kg$^{1/3}$, which resulted in a relatively small blast load. The test data are plotted in Figure 6. With the exception of P3, the pressure measurements were all less than 300 kPa. The first peak overpressure was 241.52 kPa from P5. The maximum overpressure was approximately 1.2 MPa from P3 at the apex of the model, which was mainly caused by the multiple reflections of the shock waves.

The evolution of the pressure fields inside the curved shell model could generally be deduced from the gauge data. The pressure time history curve of P3 (Figure 6(e)) shows that the shock wave first reached and crashed against the top surface of the model after the detonation. Then, the reflected

Table 1: Scheme of blast test of curved shell structure.

Scenario	TNT (g)	TNT equivalences (g)	Repeat times	Scaled distance (m/kg$^{1/3}$)
T1	5	8	1	2.850
T2	10	13	3	2.424
T3	15	18	1	2.175
T4	20	23	4	2.004

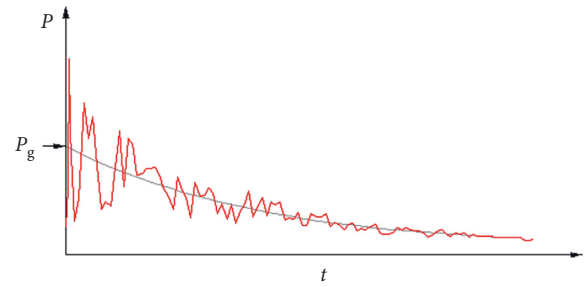

Figure 5: Gas pressure of confined blast loading (from UFC).

waves went downward and impacted the basement plane of the model. The secondary reflected waves turned around quickly and hit the top surface again. This might be one of the reasons that the tremendous shock was detected at P3; the other reasons will be explained in Section 4.1.

The data from the other gauges (Figure 6) illustrated that the shock waves reflected over and over inside the curved shell model. The peak values of the subsequent peaks at these four gauges were basically on the same level as the first peak overpressures. When some reflected waves converged together, much larger reflected waves were formed during the tests, which were less than 300 kPa. This means, for these central blast scenarios, that the middle span of a reticulated dome could easily suffer from much more severe blast actions than those at the other positions on the roof.

Moreover, it should be noted that the gauges were pair-arranged symmetrically, except for P3 on the apex of the model. However, the data from the corresponding positions were not absolutely identical. The main reasons are as follows. On one hand, the placements of the TNT charges were not on the ideal central spot of the model. On the other hand, it was impossible to record the same data using different sensors, as if recording the same input with a high-frequency signal. There were also complicated blast wave fields, with many sensitive factors.

3.2. Scenario T2. Three tests were conducted for scenario T2. However, because of spoilage during the TNT cutting process, one of the TNT charges was 1 g smaller than the others. Therefore, its results were not compared with those of the other two tests, which are presented separately in the following subsection.

Figure 7 shows the overpressure data of the first two groups for scenario T2 with 10 g of TNT. Their general trends are similar, but there are some small differences in the details.

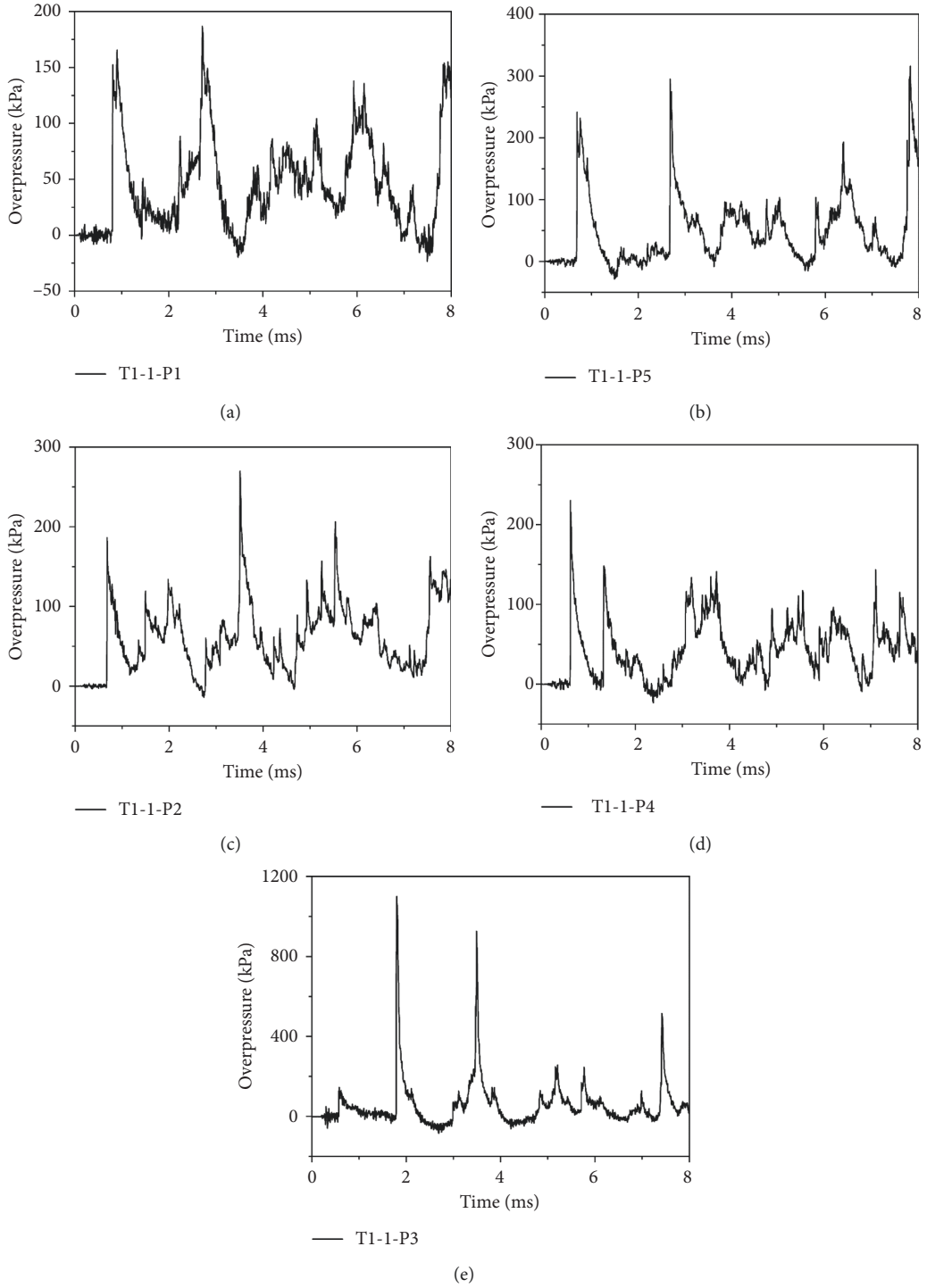

Figure 6: Experiment data from scenario T1 (8 g). (a) Test data from P1. (b) Test data from P5. (c) Test data from P2. (d) Test data from P4. (e) Test data from P3.

A comparison shows that the overpressure values from scenario T2 are evidently larger than those from scenario T1. The overpressure curves could be used to deduce that the propagation process of the blast field was similar to that for scenario T1. Because strong collisions of the shock waves occurred during the tests, some relatively large peaks were formed. The maximum overpressure was almost 3 MPa from P3. For the first overpressure peaks, P1 had the maximum value of 759.9 kPa, as shown in Figure 7(a).

In addition, the test data with 12 g of TNT are plotted in Figure 8, which shows that the overpressure values are obviously smaller than the data for the other two groups. The maximum value decreased to 1.5 MPa at P3, with that at P1 reduced to 0.5 MPa. In addition, with the TNT equivalences

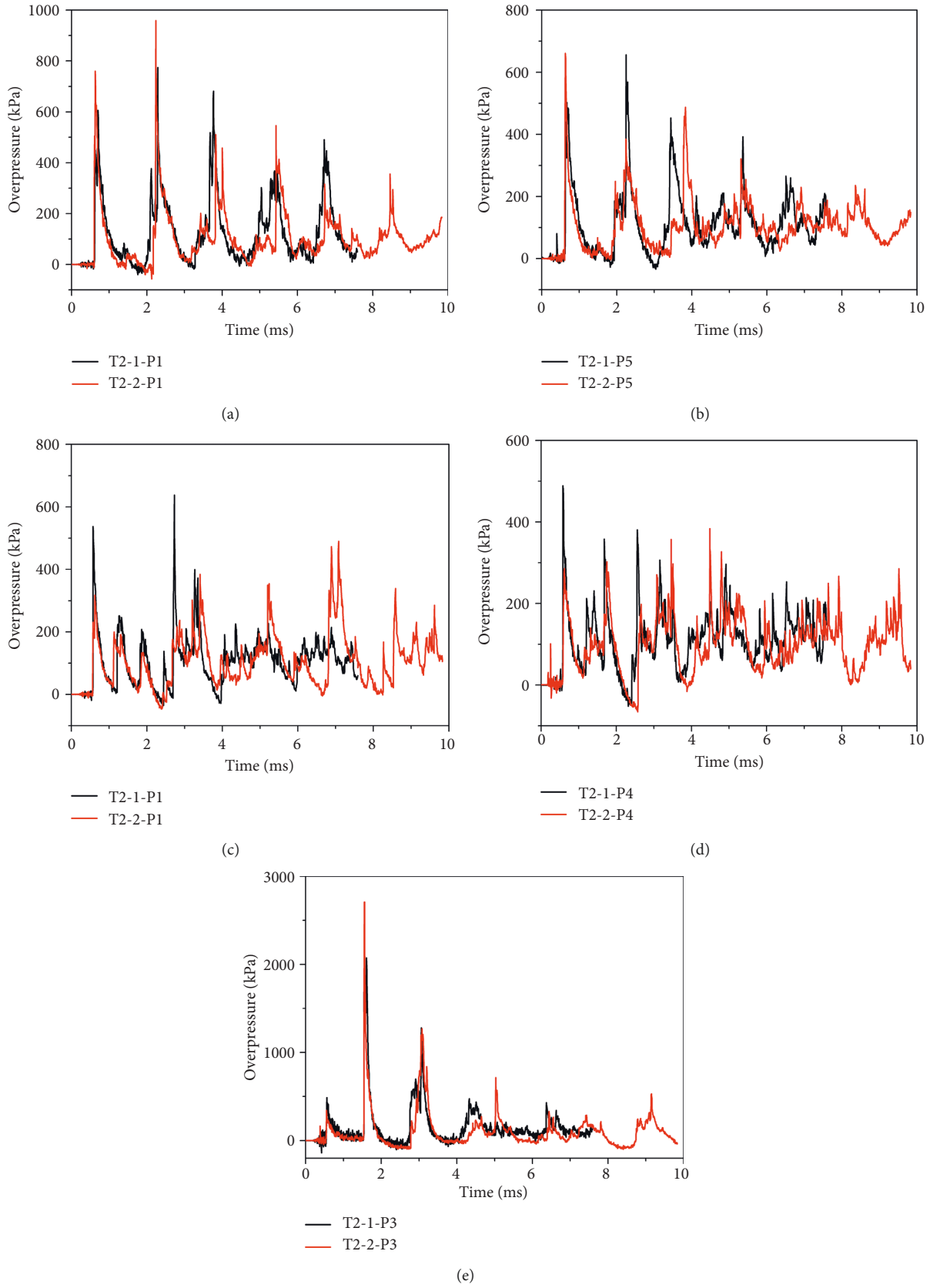

Figure 7: Experiment data from scenario T2 (13 g TNT). (a) Test data from P1. (b) Test data from P5. (c) Test data from P2. (d) Test data from P4. (e) Test data from P3.

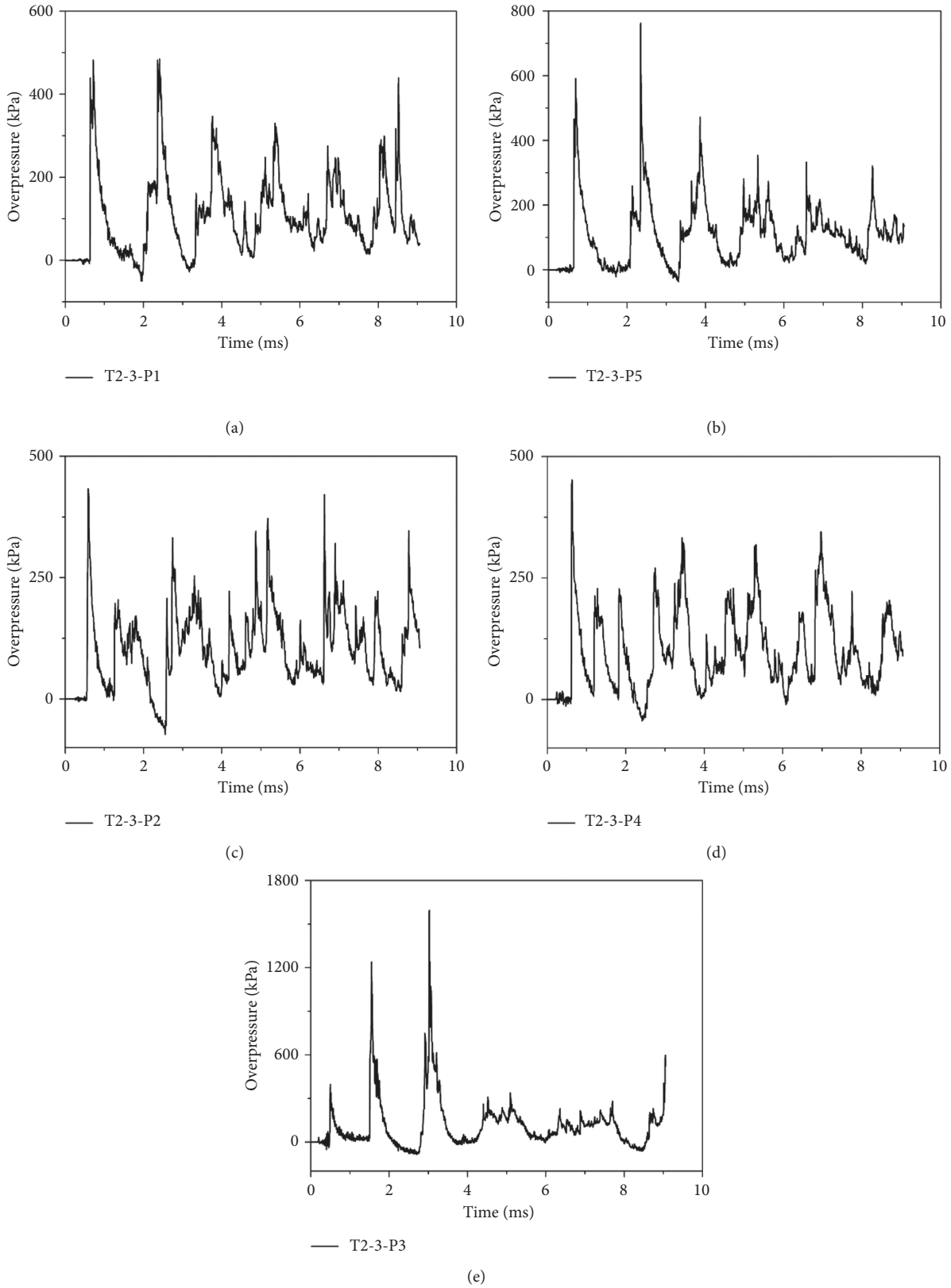

Figure 8: Experiment data from scenario T2 (12 g TNT). (a) Test data from P1. (b) Test data from P5. (c) Test data from P2. (d) Test data from P4. (e) Test data from P3.

declining, the durations of the blast pulses were much longer than those in the other two tests, for which the maximum one was almost 1 ms long.

3.3. Scenario T3. With the TNT equivalences increasing, only one experiment was conducted with 18 g because of the operation restrictions of the blast tests. The gauge data plotted in Figure 9 shows that the first peak value from P3 has obviously increased to 1000.25 kPa, which is almost on the same level as the second and third peaks. Moreover, the durations are much shorter than the above data, with only 0.47 ms for P3, almost half that of the durations of the above tests. This means that the waves reflected from different directions were coincidently superimposed together, which could still be recognized as a slight time delay on the recorded curve. In addition, in this scenario, the maximum first peak value is 1002.42 kPa from P1, which is slightly larger than that of P3.

3.4. Scenario T4. Four blast tests were conducted with scenario T4. However, the explosives were not detonated completely. Some black explosive residue was left on the basement plane when the shell model was removed after the tests, as shown in Figure 10. Moreover, the records from these two tests show distinctly lower values than the others. Thus, they were treated as valid data but are not presented in this paper.

The overpressure curves in Figure 11 show that good agreement was achieved between the other two tests, especially on the arrival time of the peak overpressures, with a slight difference in the values. The maximum first peak value of 1355.36 kPa came from P5.

3.5. Summary of Test Data. In this subsection, the above test data are compared quantificationally. Complicated propagations and reflections of the blast waves occurred during the interior blast tests. Therefore, the maximum peak values from the tests are important, but there is no meaning to a comparison with other test data. This is because sometimes two or more reflected waves merged together coincidentally, which resulted in the maximum reflected value. However, the first peak pressure values from the tests could carry more useful information directly. All of the first peak overpressure data from each scenario are listed in Table 2.

With an increase in the TNT equivalence, the peak pressure values rapidly increased. However, with this general trend, the record of 1000.25 kPa for scenario T3 from P3 is special, because it is obviously larger than those of scenario T4. Table 3 lists the impulses of the first 5 ms blast loading data. The increasing trends are much more obvious in these data and could explain the abnormal value for scenario T3. The abnormal value could be related to two reflected peaks merging coincidently and being recognized as one.

4. Numerical Model and Verification

It should be noted that although the general trends for the overpressure curves are consistent for the same scenario, the peak values are not identical. The main reasons for these differences are related to the TNT equivalences and positions. The blast propagation and reflection from an interior surface is a complicated process. A tiny variation should lead to an evident difference in the results. However, it would be impossible to see what happened inside the shell model even if high-speed cameras were used because of the fireball and smoke during the blast tests. A numerical simulation is the best way to determine what occurs inside the shell model, and it could be repeated many times with different scenarios without the high costs of blast tests.

The blast propagation medium should be modelled in numerical simulation studies. However, three-dimensional models are extraordinarily large. This not only makes them time-consuming to utilize, but also lowers the precision because of the computing power limitation, which is not suitable for a parametric analysis.

Consequently, a simplified method is proposed in this paper based on the features of this problem. The inner space of the rigid shell model is symmetric, with a central axis, as shown in Figure 12(a). In addition, the explosives are detonated in the center at ground level in all the scenarios referenced above. The three-dimensional model could be simplified into a two-dimensional model using the AUTODYN software package [20], as shown in Figure 12(b).

Euler elements were adopted to set up the numerical model. A three-dimensional model could be obtained by rotating the two-dimensional model around the symmetry axis. The other boundaries were all rigid to consider the restriction of the 30 mm steel shell. In addition, to simulate the detonation platform in the middle of the basement plane (Figure 13), the unused elements in AUTODYN were adopted to refine the rigid boundaries.

The Jones–Wilkins–Lee (JWL) equation of state was used to simulate the TNT detonation process, which is expressed as follows [20].

$$p = C_1\left(1 - \frac{\omega}{r_1 v}\right)e^{-r_1 v} + C_2\left(1 - \frac{\omega}{r_2 v}\right)e^{-r_2 v} + \frac{\omega e}{v}, \quad (2)$$

where C_1, r_1, C_2, r_2, ω, and v are constants, with the specific values listed in Table 4.

The ideal gas equation of state was used to simulate the propagation medium of air [20], which could be expressed as the Gay–Lussac equation.

$$p = (\gamma - 1)\rho e, \quad (3)$$

where ρ is the density of air, and γ is a constant equal to 1.4.

The four scenarios of the blast tests were simulated using the parameters and model above. Good agreement was found in comparisons. Taking scenario T2 and T4 as examples, comparisons of the results of the tests and numerical simulations are presented in the following subsections.

4.1. Simulation of Scenario T2. Taking the simulation of scenario T2 as an example, the detonation and propagation processes are shown in Figure 14. It can be seen that the TNT detonated in the center of the shell, and the spherical shock

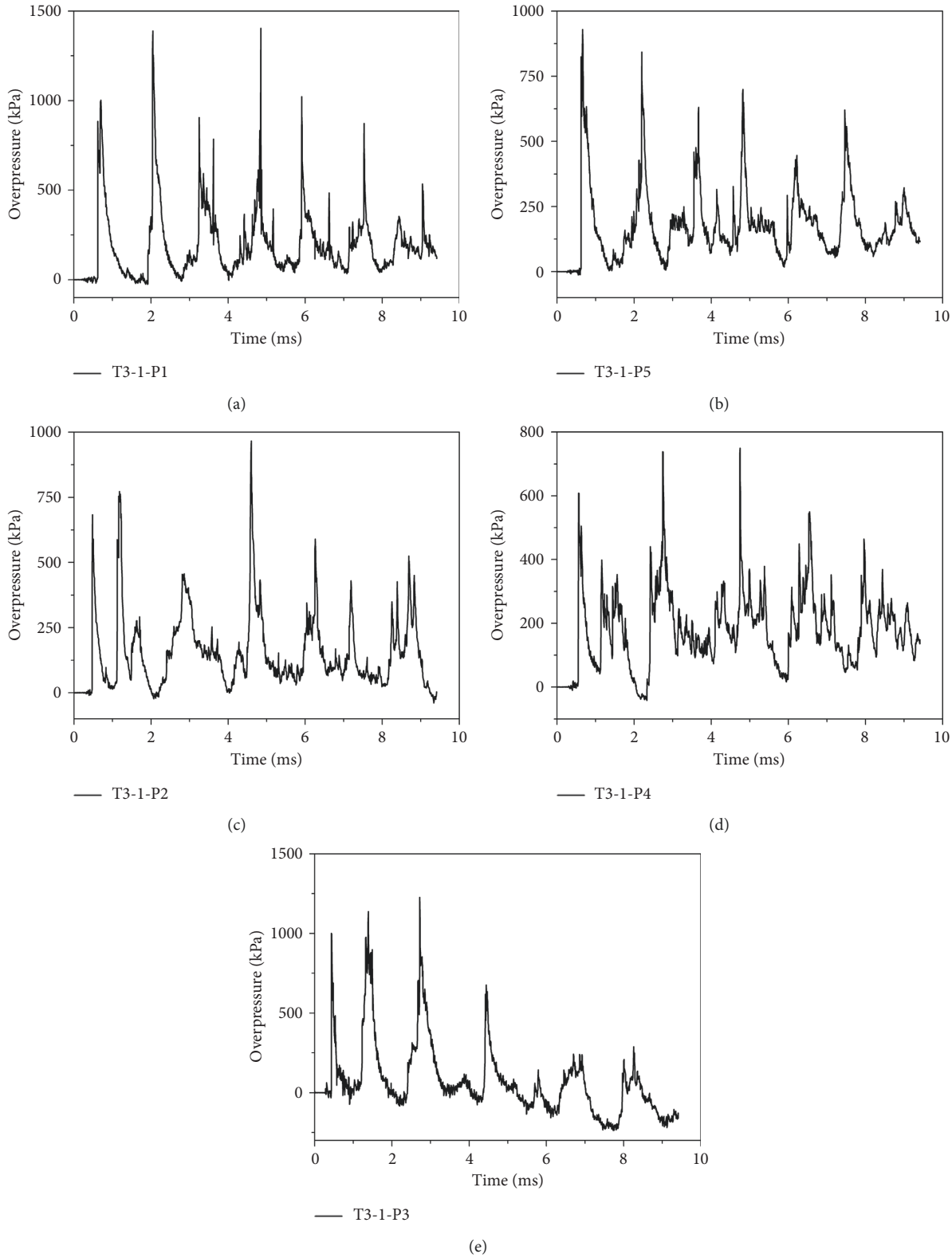

Figure 9: Experiment data from scenario T3 (15 g TNT). (a) Test data from P1. (b) Test data from P5. (c) Test data from P2. (d) Test data from P4. (e) Test data from P3.

waves quickly swelled, as shown in Figures 14(a) and 14(b). The blast first crashed into and reflected of the side wall of the shell, and then reached the top of the roof (Figure 14(c)). Reflected waves were generated and continually propagated to different positions. At the same time, the first shock wave directly generated from the TNT also arrived at the junction

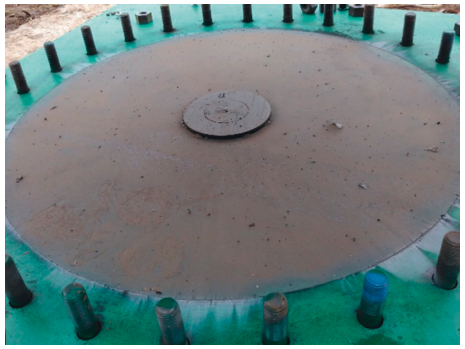

Figure 10: Residue from TNT after explosion.

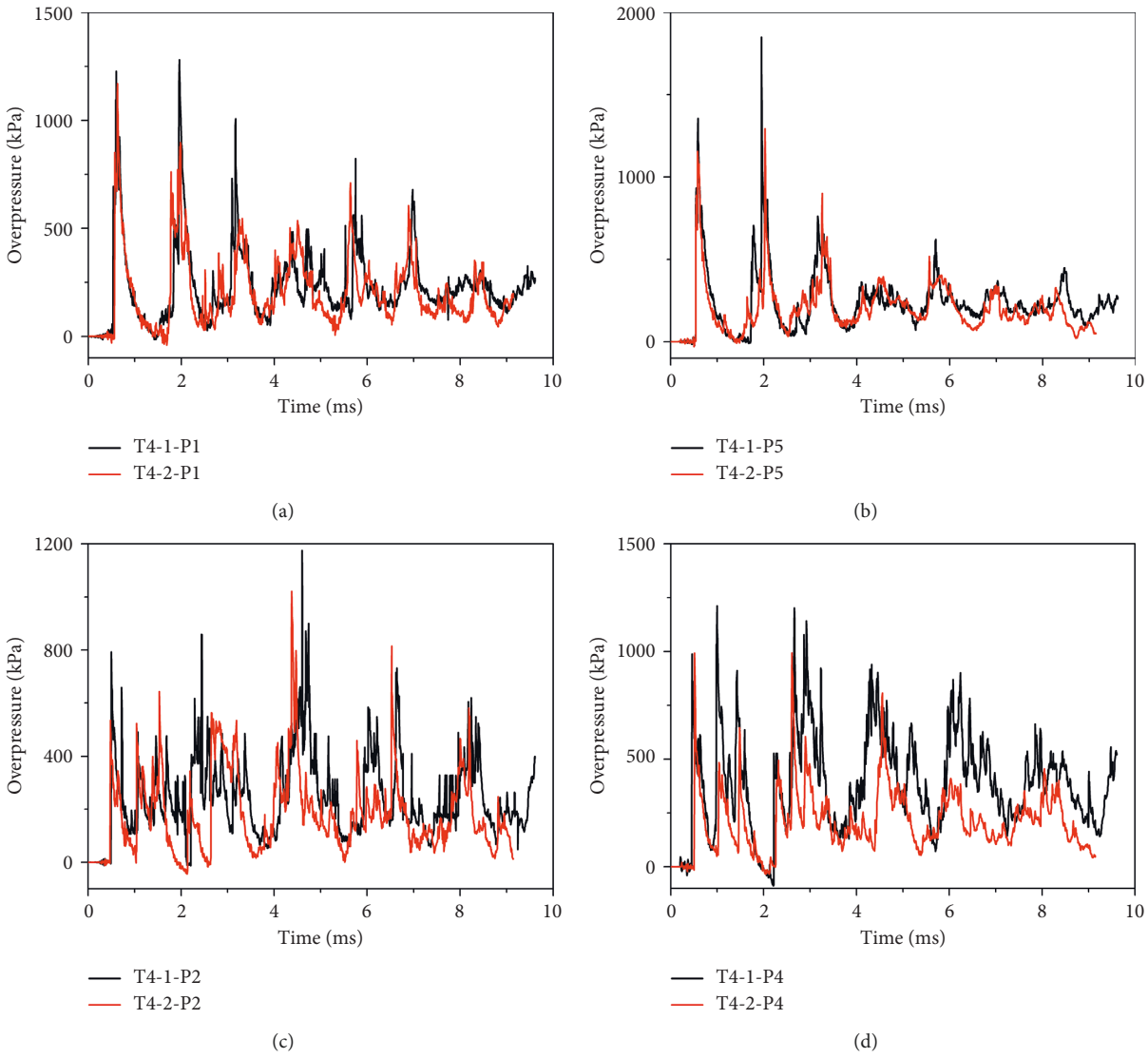

Figure 11: Continued.

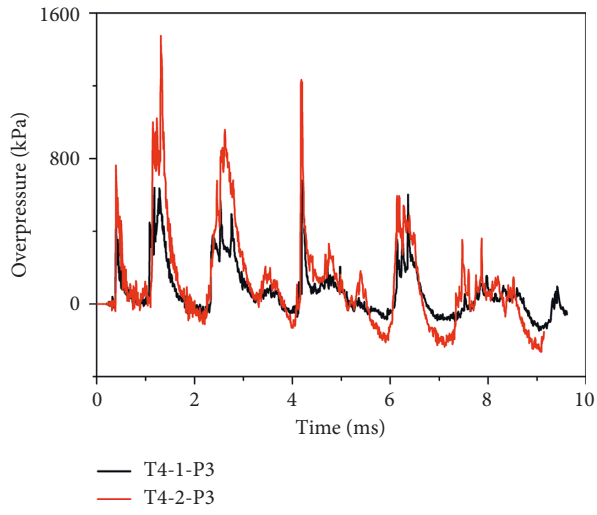

(e)

Figure 11: Experiment data from scenario T4 (20 g TNT). (a) Test data from P1. (b) Test data from P5. (c) Test data from P2. (d) Test data from P4. (e) Test data from P3.

Table 2: First peak overpressure from each scenario (units: kPa).

	5 g		10 g	15 g		20 g
P1	152.46	482.38	759.9	1002.42	1170.22	1227.2
P2	186.69	433.45	317.23	682.77	534.88	792.32
P3	145.85	396.75	342.27	1000.25	762.32	518.53
P4	230.29	451.64	285.89	608.37	992.37	988.89
P5	241.52	591.55	660.72	928.86	1155.99	1355.36

Table 3: Impulse from each scenario (units: kPa·ms).

	5 g		10 g	15 g		20 g
P1	205.81	546.15	768.82	971.87	961.60	1176.49
P2	256.59	488.07	749.81	845.14	890.15	1252.48
P3	355.98	845.61	803.16	833.44	980.25	573.18
P4	191.63	493.13	670.97	846.10	875.14	1873.52
P5	226.32	530.91	747.77	871.52	933.15	1192.69

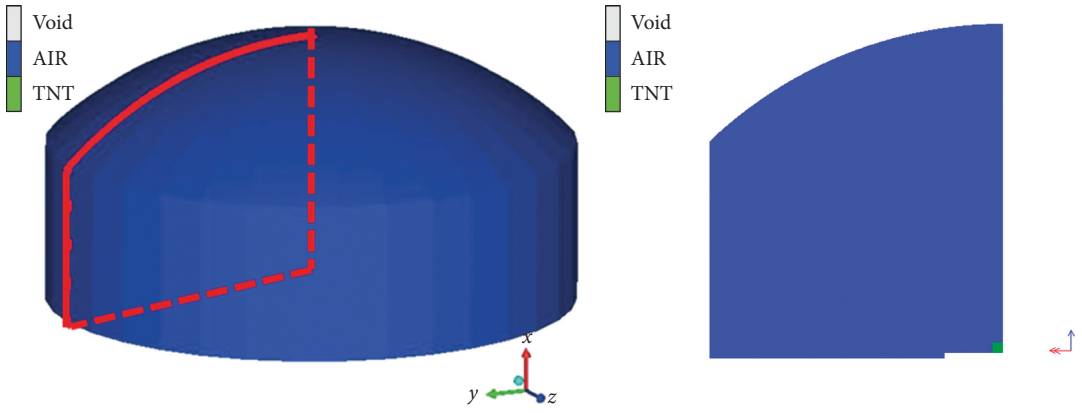

(a) (b)

Figure 12: Simplified model for blast loading in curved shell structures. (a) 3D numerical model, and (b) 2D simplified numerical model.

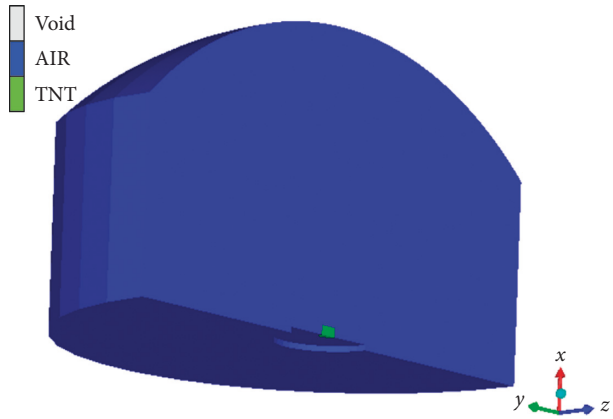

Figure 13: Equivalent 3D model with detonation platform.

Table 4: Parameters of TNT.

C_1 (GPa)	C_2 (GPa)	r_1	r_2	ω	v (m/s)
374	3.75	4.15	0.90	0.35	6930

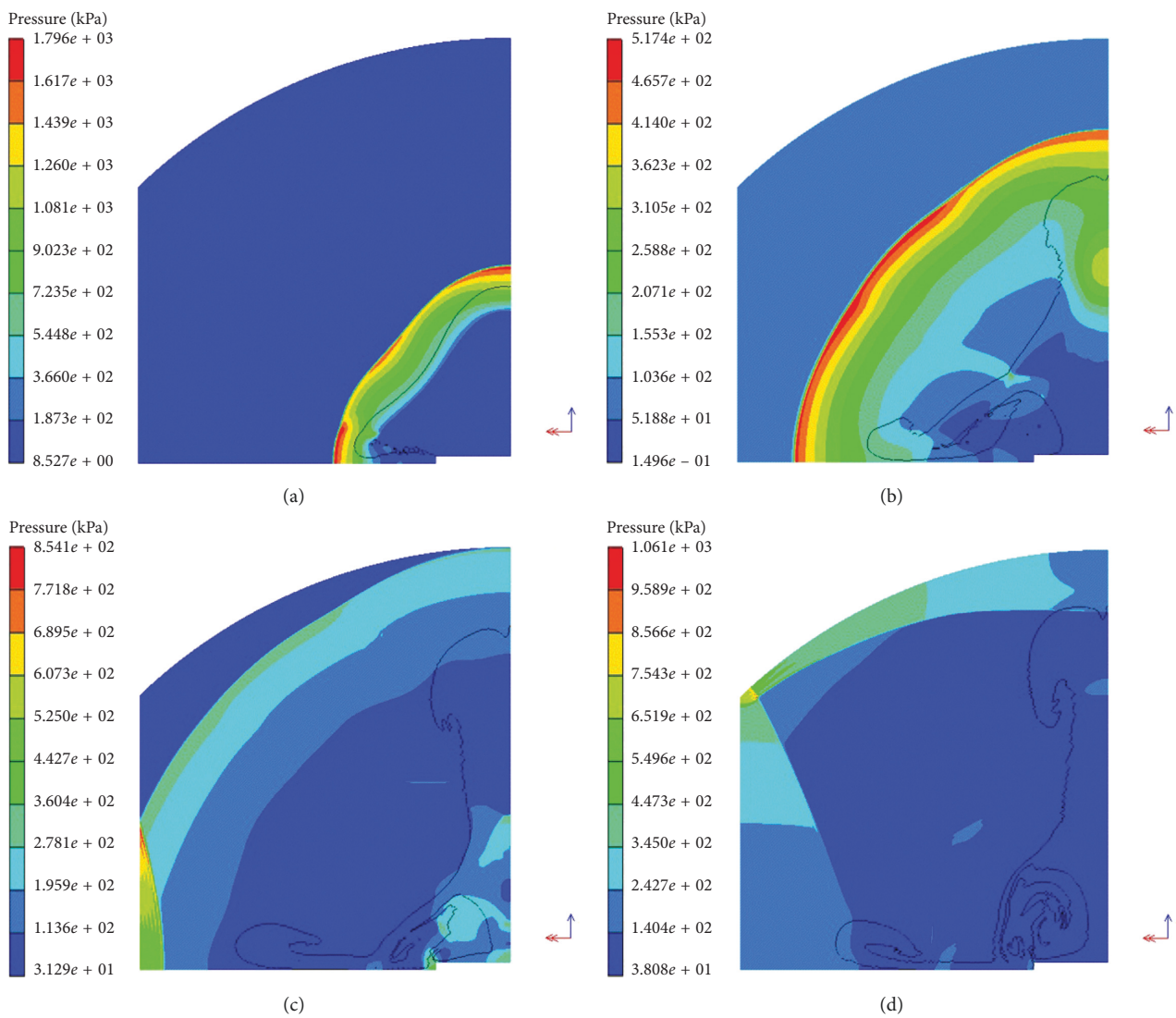

Figure 14: Continued.

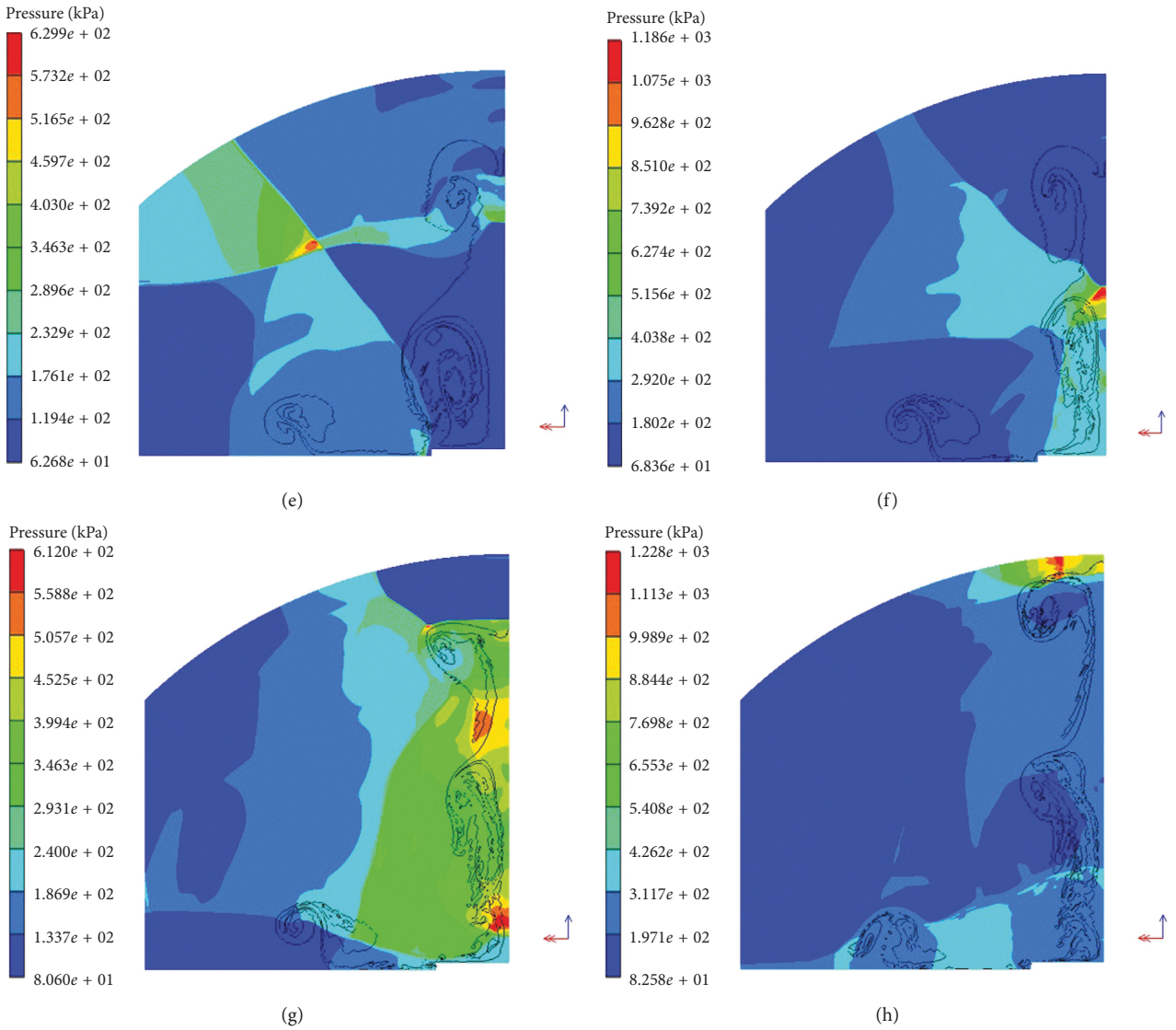

Figure 14: Evolution of pressure field in curved structure. (a) 0.1 ms. (b) 0.3 ms. (c) 0.5 ms. (d) 0.7 ms. (e) 1.0 ms. (f) 1.2 ms. (g) 1.4 ms. (h) 1.6 ms.

between the roof and wall. These waves merged together and formed a new reflected wave (Figure 14(d)). This new reflected wave rushed downward (Figures 14(e) and 14(f) and encountered a wave reflected from the ground, which generated the largest peak pressure on the top of the shell at position P3, as shown in Figures 14(g) and 14(h)).

The overpressure data from the specific positions of the gauges were output and plotted in the same figure to compare with the test data in Figure 15. The overpressure curves are plotted with solid lines, with dashed lines used for the impulses, which were obtained by the integral of the overpressure data. In addition, the black and red lines represent the test data, and the blue lines are the simulation results.

From Figure 15, the simulation results are consistent with the test data from the blast tests. Especially for the first reflected peak, both the arrival times and shapes are the same as those of the gauge recordings. The subsequent reflected peaks of the numerical simulations are slightly smaller than those of the tests, while the arrival times of the subsequent peaks are close to those of the tests. This is mainly because the JWL equation of state cannot account for the energy of the afterburning effect [21, 22], which involves a series of complicated chemical reactions, including some additional combustion processes of C, CO, H_2, and so on. Moreover, the afterburning process occurred after the detonation, which means the first values of reflected peaks were not affected.

4.2. Simulation of Scenario T4. In comparison to the test data of scenario T4, the simulation results had good agreement with P1 and P5. As shown in Figure 16(a), the simulation could well demonstrate the features of the whole trend, peak reflected values, impulses, and arrival times for the first reflected wave. However, the results of comparisons for

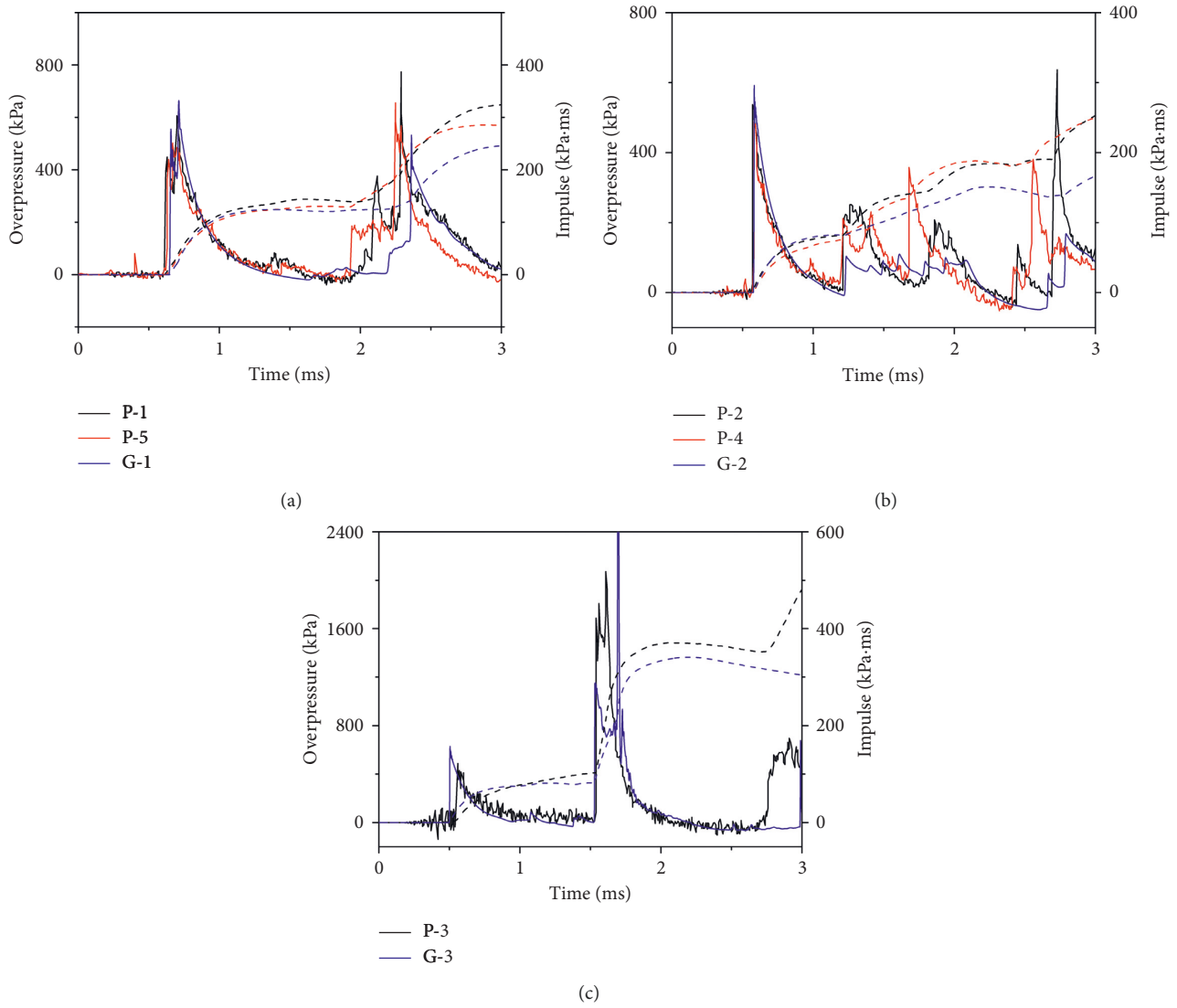

Figure 15: Comparisons between test data and numerical simulation data for scenario T2. Comparison between (a) test and simulation (P1 & P5), (b) test and simulation (P2 & P4), and (c) test and simulation (P3).

positions P2 and P4 were not as good (Figure 16(b)). On the one hand, the results of the test data had a distinct difference, with the recording from P2 obviously smaller than that of P4. On the other hand, there was a double peak for the first reflected peak of P2. This might have been caused by the original fixed position of the TNT, which was quite sensitive to the pressure fields. Because the positions of P1 and P5 were much further away, the asymmetrical effects were not as obvious. From Figure 16(c), it can be seen that the test data are slightly smaller than the data of the simulations for the first reflected peak, as well as for the second one. However, the general trends are quite similar.

In addition, it should be noted that the explosives used in the numerical simulations had hemispherical shapes because of the limitations of the 2D model. However, TNT cubes were used in the blast tests, because these were much easier to cut. The effects of charge shapes are mainly reflected in the near field of blast. The study in this paper focused on the interior blast loading of large-span spatial structures, of which the cases in this study are relating to far-field issues. Therefore, in order to simplify the simulation procedure, the hemispherical TNT was used. From the comparison results, it also illustrates that the effect of the TNT shape is not very important with a relatively large-scaled distance.

From the above comparisons of the simulation and test results for two scenarios, it can be determined that the numerical simulation methods and parameters in AUTODYN are suitable for considering this interior blast problem and could be used for predicting the blast field in a shell structure.

5. Prediction from Parameter Analysis

The previously discussed blast tests and numerical simulations showed that the prediction process for blast loading is complicated, making it inconvenient for engineers during

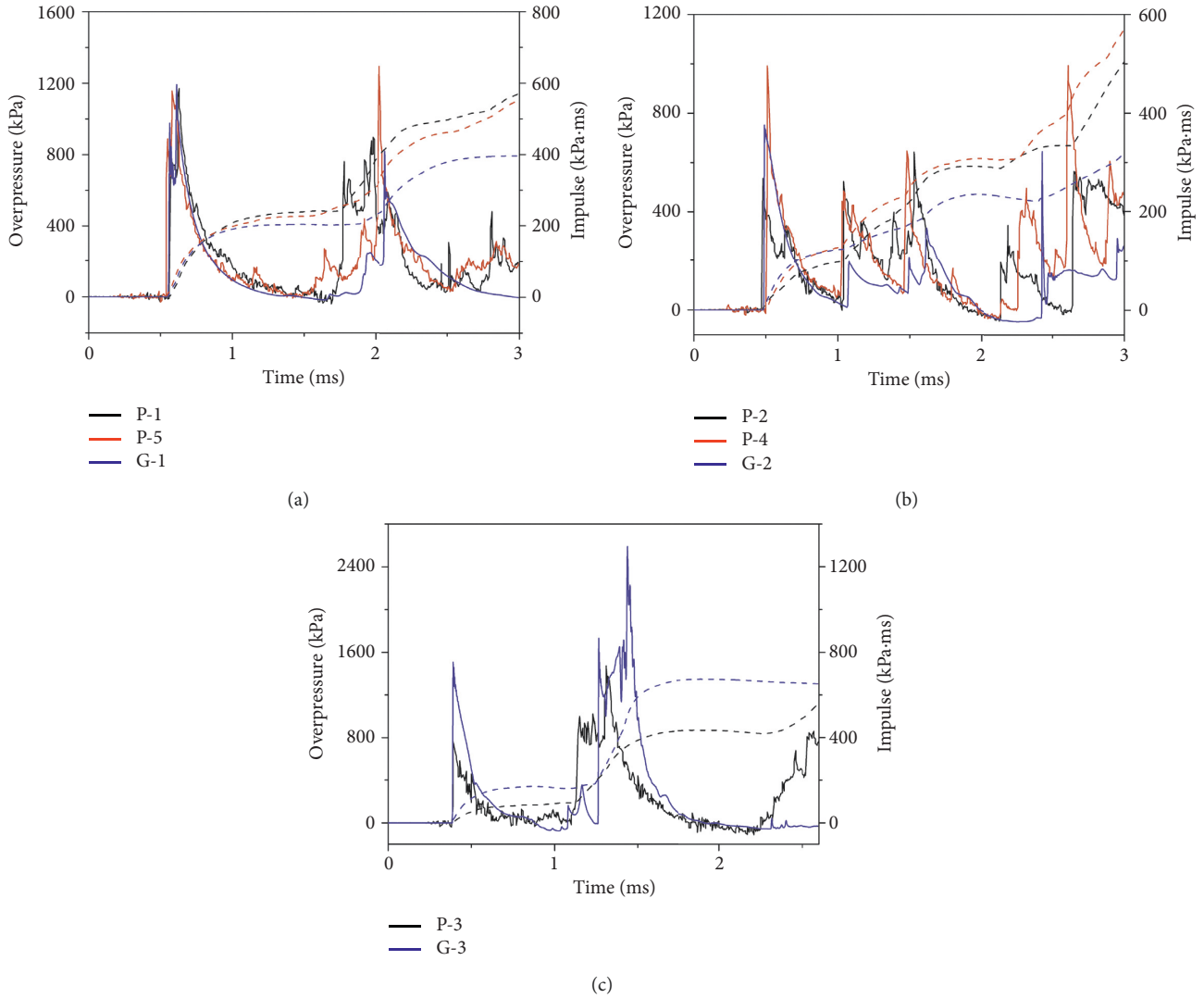

Figure 16: Comparisons between test data and numerical simulation data of scenario T4. Comparison between (a) test and simulation (P1 & P5), (b) test and simulation (P2 & P4), and (c) test and simulation (P3).

the design period. However, most reticulated domes have similar interior spaces enclosed with a roof system, support walls, and a ground floor, which means the blast loading distributions follow similar rules. Therefore, based on the similarity law, a detonation would generate self-similar blast waves on the same-scaled distance within geometrically similar environments, which represents a much simpler way to obtain the blast field. This means, as shown in Figure 17, that two spherical charges would generate blast loads with certain relations, which include the same peak pressures. In addition, both the impulses and durations differ by a factor of k, where k is a constant based on the relationship between the dimensions of the two charges. Consequently, the blast loading of a long-spatial structure could be deduced from a similar small model based on the similarity law [23].

A system parametrical analysis was conducted with a 10 m span model. According the convergence analysis in reference [16], 300-element in the radial direction of the model is a suitable meshing scheme for this problem. The 2D

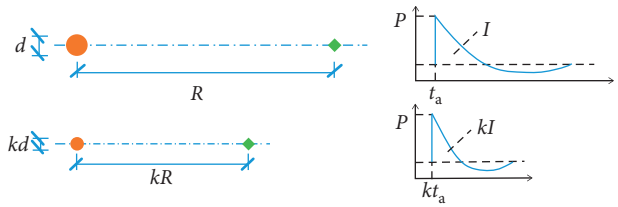

Figure 17: Similarity law of blast.

model in the following sections includes more than 0.1 million Euler cells, which are ranging from 6 mm to 16 mm.

By analyzing the distribution rules of blast loading, three key parameters, varying rise-span ratio f/L, height-span ratio H/L, and scaled distance Z, were distinguished as the most influential ones. The blast loading on the interior surfaces from parametrical analysis of the model are listed in Tables 5–7.

Table 5: Results of parameter analysis with different scaled distances.

Z (m·kg$^{-1/3}$)	2.3		2.5		2.9		4		5	
	I (kPa·ms)	P (kPa)	I (kPa·ms)	P (kPa)	I (kPa·ms)	P (kPa)	I (kPa·ms)	P (kPa)	I (kPa·ms)	P (kPa)
Top	1017.5	750.4	835.4	590.9	571.7	382.9	276.9	181.0	165.5	111.1
Corner	689.3	713.7	566.5	569.6	384.4	377.5	172.7	178.9	97.3	110.0

Table 6: Results of parameter analysis with different rise-span ratios.

f/L	0		0.125		0.2		0.25		0.5	
	I (kPa·ms)	P (kPa)	I (kPa·ms)	P (kPa)	I (kPa·ms)	P (kPa)	I (kPa·ms)	P (kPa)	I (kPa·ms)	P (kPa)
Top	718.5	467.4	646.4	386.8	571.7	382.9	538.4	397.0	522.7	387.6
Corner	296.9	399.3	359.5	398.1	384.4	377.5	417.0	378.0	526.5	395.5

Table 7: Results of parameter analysis with different height-span ratios.

H/L	0.4		0.45		0.5		0.55		0.6	
	I (kPa·ms)	P (kPa)	I (kPa·ms)	P (kPa)	I (kPa·ms)	P (kPa)	I (kPa·ms)	P (kPa)	I (kPa·ms)	P (kPa)
Top	345.3	253.5	458.0	310.4	571.7	382.9	680.8	398.5	813.8	474.5
Corner	249.1	375.2	328.0	381.4	384.4	377.5	469.0	377.1	564.8	380.2

This study is aimed on dealing with the blast loading for a wider scope of spatial structures, of which the specific intershapes are various. Therefore, a series of simulations were conducted for those typical intershapes of spatial structures in Tables 5–7. By using the method proposed in reference [16], the data obtained from the standard models could be used to deduce similar blast distributions for large-span structures. Therefore, the blast loads of other issues could be predicted quickly with these similar data without executing blast tests and simulations. The predicted blast loading could be used as the suggestion for structural design.

6. Conclusions

Confined blast tests were conducted with an almost rigid curved shell model to determine the blast pressure fields within a reticulated dome. The blast data of the pressure-time histories were recorded using PCB gauges at five typical positions. Four scenarios with different TNT equivalences were used, and the pressure fields in the curved shell model were compared. The overpressures and impulses of the first peak for each scenario were compared and studied. The results showed that the first peaks had obvious regularity when the TNT equivalence was changed, whereas the subsequent blast loading peaks did not, which was caused by the complicated evolution process for the shock wave fields in the confined blast. In addition, a simplified method for the numerical simulation of blast loading was introduced. The blast scenarios were simulated and verified using the test data. The dynamic evolution of the blast propagation and reflection processes was effectively explored by the numerical simulations, with the contour plots observed in detail using AUTODYN. Finally, a parameter analysis of the blast loading was conducted with some key parameters varied within a reasonable scope. Based on these results, the interior blast loading at the important positions of other reticulated domes could conveniently be predicted using the existing data, which could be used in the protective design and rapid assessment of the reticulated domes.

Data Availability

The data used to support the findings of this study are available from the corresponding author upon request.

Conflicts of Interest

The authors declare that they have no conflicts of interest.

Acknowledgments

The research presented in this paper was jointly supported by the National Natural Science Foundation of China (grant no. 51708521) and Foundation of Key Laboratory of Structures Dynamic Behavior and Control (Ministry of Education) in Harbin Institute of Technology of China (grant no. HITCE201803). The first author would also like to express the sincere acknowledgements to Prof. Yadong Zhang and Hengbo Xiang for their suggestions and help on the blast tests.

References

[1] UFC 3-340-02, *Structures to Resist the Effects of Accidental Explosions*, UFC, Departments of the Army, the Navy, and the Air Force, Las Vegas, NV, USA, 2008.

[2] Y. Hu, C. Wu, M. Lukaszewicz, J. Dragos, J. Ren, and M. Haskett, "Characteristics of confined blast loading in unvented structures," *International Journal of Protective Structures*, vol. 2, no. 1, pp. 21–43, 2011.

[3] C. Wu, M. Lukaszewicz, K. Schebella, and L. Antanovskii, "Experimental and numerical investigation of confined

explosion in a blast chamber," *Journal of Loss Prevention in the Process Industries*, vol. 26, no. 4, pp. 737–750, 2013.

[4] C. Wu, G. Fattori, A. Whittaker, and D. J. Oehlers, "Investigation of air-blast effects from spherical-and cylindrical-shaped charges," *International Journal of Protective Structures*, vol. 1, no. 3, pp. 345–362, 2010.

[5] C. Wu and H. Hao, "Modeling of simultaneous ground shock and airblast pressure on nearby structures from surface explosions," *International Journal of Impact Engineering*, vol. 31, no. 6, pp. 699–717, 2005.

[6] S. Yang, Q. Fang, Y. Zhang et al., "A numerical method of calculating the consequence of heterogeneous mixed vapor cloud explosion," *Natural Gas Industry*, vol. 34, pp. 155–161, 2014, in Chinese.

[7] Q. Bao, Q. Fang, Y. Zhang, L. Chen, S. Yang, and Z. Li, "Effects of gas concentration and venting pressure on overpressure transients during vented explosion of methane-air mixtures," *Fuel*, vol. 175, pp. 40–48, 2016.

[8] Z. Li, Y. Shi, and H. Zhou, "Propagation law and overpressure load of blast wave in urban compels environment," *Engineering Mechanics*, vol. 26, pp. 178–183, 2009.

[9] Y. Shi, Z. Li, and H. Hao, "Mesh size effect in numerical simulation of blast wave propagation and interaction with structures," *Transactions of Tianjin University*, vol. 14, no. 6, pp. 396–402, 2008.

[10] Y. Shi, Z.-X. Li, and H. Hao, "A new method for progressive collapse analysis of RC frames under blast loading," *Engineering Structures*, vol. 32, no. 6, pp. 1691–1703, 2010.

[11] Y. Shi, H. Hao, and Z. Li, "Numerical simulation of blast wave interaction with structure columns," *Shock Waves*, vol. 17, no. 1-2, pp. 111–123, 2007.

[12] X. Gao and S. Wang, "Deflection of architectural laminated glasses under static and explosive loads," *Journal of the Chinese Ceramic Society*, vol. 36, pp. 1477–1483, 2008.

[13] Z. Xudong, Q. Shaobo, F. Feng, and Z. Ximei, "Experimental and numerical investigations of a single-layer reticulated dome subjected to external blast loading," *Engineering Structures*, vol. 176, pp. 103–114, 2018.

[14] X.-B. Zhi, S.-B. Qi, and F. Fan, "Temporal and spatial pressure distribution characteristics of hemispherical shell structure subjected to external explosion," *Thin-Walled Structures*, vol. 137, pp. 472–486, 2019.

[15] J. Ma, Z. Xudong, and F. Fan, *The Study on Loading Field of Inner Blast inside the Shells*, The 13rd IASS Conference, Shenzhen, China, 2010, in Chinese.

[16] J. L. Ma, C. Q. Wu, X. D. Zhi, and F. Fan, "Prediction of confined blast loading in single-layer lattice shells," *Advances in Structural Engineering*, vol. 17, no. 7, pp. 1029–1043, 2014.

[17] J. Ma, F. Fan, C. Wu, and X. Zhi, "Counter-intuitive collapse of single-layer reticulated domes subject to interior blast loading," *Thin-Walled Structures*, vol. 96, pp. 130–138, 2015.

[18] J. Ma, F. Fan, L. Zhang, C. Wu, and X. Zhi, "Failure modes and failure mechanisms of single-layer reticulated domes subjected to interior blasts," *Thin-Walled Structures*, vol. 132, pp. 208–216, 2018.

[19] W. E. Baker, *Explosions in Air*, University of Texas Press, Austin, TX, USA, 1973.

[20] Century Dynamics, *AUTODYN Theory Manual, Revision*, Vol. 4, Century Dynamics, Concord, CA, USA, 2005.

[21] I. Edri, V. R. Feldgun, Y. S. Karinski, and D. Z. Yankelevsky, "Afterburning aspects in an internal TNT explosion," *International Journal of Protective Structures*, vol. 4, no. 1, pp. 97–116, 2013.

[22] I. Edri, V. R. Feldgun, Y. S. Karinski, and D. Z. Yankelevsky, "On blast pressure analysis due to a partially confined explosion: III. Afterburning effect," *International Journal of Protective Structures*, vol. 3, no. 3, pp. 311–331, 2012.

[23] J. Henrych, *The Dynamics of Explosion and its Use*, Elsevier Scientific Pub. Co., Amsterdam, Netherlands, 1979.